Numerical Studies of Hall Thruster Acceleration Region Electron Transport

Ira Katz,[1] Vernon H. Chaplin Jr.[2], and Alejandro Lopez Ortega[3]
Jet Propulsion Laboratory, California Institute of Technology, Pasadena, CA, 91107, USA

Azimuthal direction 1-D and azimuthal and axial direction 2-D Particle in Cell (PIC) simulations of the Hall thruster acceleration and near-plume regions are presented. The axial extent of the 2-D computational domain is based on the ExB drift parameter, D_{ExB}, the number of times around the channel an electron ExB drifts before being scattered. With only high energy main beam ions, the simulations produced a broad potential profile in the acceleration region. The addition of a small amount of ionization in the acceleration domain at a rate consistent with Hall thruster parameters causes the potential profile to develop two distinct regions. In the upstream portion of the computational domain, the potential profile is very steep, typical of Hall thruster acceleration regions. In the downstream portion, the potential profile is almost flat, like potentials in Hall thruster near plume regions. This bifurcation happens naturally; there is no other change in code parameters between the two results. Without the addition of a small amount of ionization in the acceleration region, the axial electron transport is very low. With ionization, the calculated ratio of electron current to ion current is the same order of those measured in Hall thrusters. This suggests that in regions with lower energy electrons and ions, plasma waves are effective in allowing cross-field transport, and axial electric fields are small. In the acceleration region, the plasma waves are less effective at scattering the energetic electrons, and high axial electric fields are needed to produce the observed cross-field electron transport.

I. Nomenclature

$\mathbf{B}$	=	magnetic field vector
$\bar{c}$	=	electron thermal speed
D_{ExB}	=	ExB drift parameter
dt	=	time step
$\mathbf{E}$	=	electric field
j_e	=	electron current density
j_i	=	ion current density
m_e	=	electron mass
m_{Xe}	=	xenon ion mass
n_e	=	electron number density
n_{Xe}	=	xenon ion number density
ν_{class}	=	classical electron scattering frequencies
ν_{en}, ν_{ei}	=	classical electron neutral and electron ion scattering frequency
ϕ	=	plasma potential
$R_{thruster}$	=	radius of the Hall thruster annular channel
r	=	radial dimension
T_e	=	electron temperature

[1] Principle Engineer, Propulsion and Materials Engineering Section, 4800 Oak Grove Dr., Pasadena, CA 91109, MS 125-109, AIAA Senior Member.

[2] Member of the Technical Staff, Electric Propulsion Group, 4800 Oak Grove Dr., Pasadena, CA 91109, MS 125-109.

[3] Member of the Technical Staff, Electric Propulsion Group, 4800 Oak Grove Drive, Pasadena, CA, 91109, MS 125-109, Member AIAA.

θ, y	=	azimuthal dimension
$\mathbf{u}$	=	electron velocity
z	=	axial dimension
Ω	=	Hall parameter
ω_{ce}	=	electron cyclotron frequency

II. Introduction

Hall effect thrusters are closed drift, crosse-field devices used for spacecraft propulsion. The physics controlling electron transport in Hall thrusters has been the subject of intense study for decades. Figure 1 shows an operating Hall thruster and the coordinate system used in this paper. There have been two major approaches to modeling Hall thruster plasmas. The first, 1-D axial and 2-D r-z, codes [1-6] take advantage of the axial symmetry of most Hall thrusters. While the codes differ in how they model ions, they all model the electrons as a Maxwellian fluid. The weakness in this approach is that classical collisions are insufficient to account for the observed electron currents. To overcome this, ad hoc, experimentally informed "anomalous", collision profiles are necessary to reproduce the electron currents and potential profiles observed in Hall thrusters. These codes reproduce thruster plasmas well enough that they are used as design tools, and predict quantities such as plume profiles, channel erosion [7,8], propellant utilization, and thrust. Calculations using one of these codes, Hall2De, provided the insight that led to the discovery of magnetic shielding, which has enabled the design of long life Hall thrusters [9, 10].

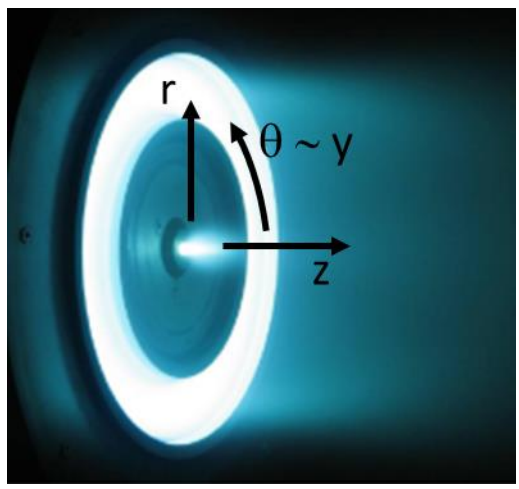

Fig. 1 A Hall thruster creates ions in an annular channel with an axial (z) electric field and a radial (r) magnetic field. Electrons ExB drift in the azimuthal (θ) direction

We use output from a Hall2De calculation to illustrate the ion and electron flows and potential profile typical of Hall thrusters. Hall2De calculated potentials and electron scattering frequencies along a thruster channel centerline are shown in Figure 2. Typical of all Hall thrusters, the potential doesn't drop uniformly from the anode to the cathode, but rather drops precipitously over a short distance between two longer regions of relatively low electric field.

Hall2De assumes fluid electrons and solves Ohm's law for the electric potential. The conductivity includes both classical scattering, calculated self-consistently in the code, and an ad hoc, experimentally informed, "anomalous" scattering profile. The eventual goal of our research is to replace the ad hoc profile in Hall2De with a model generated self-consistently from the code's calculated plasma parameters.

Throughout this paper, we refer to three axial regions of Hall thrusters shown in Figure 2: the anode ionization region, the acceleration region, and the near plume region. Neutral gas flowing out of the anode is ionized upstream in the anode ionization region. Axial electric fields are low. Classical, electron-neutral and electron-ion scattering, dominate in this region. Once the ions fall through a few volts, classical scattering becomes less important. The acceleration region is characterized by strong axial electric fields and non-classical, anomalous transport. Downstream in the near plume region, the axial electric fields drop considerably and the potential profile is almost flat. The magnetic field is still relatively high. The low electric field can only be explained by anomalous transport; classical scattering is orders of magnitude too small to account for the low electric field.

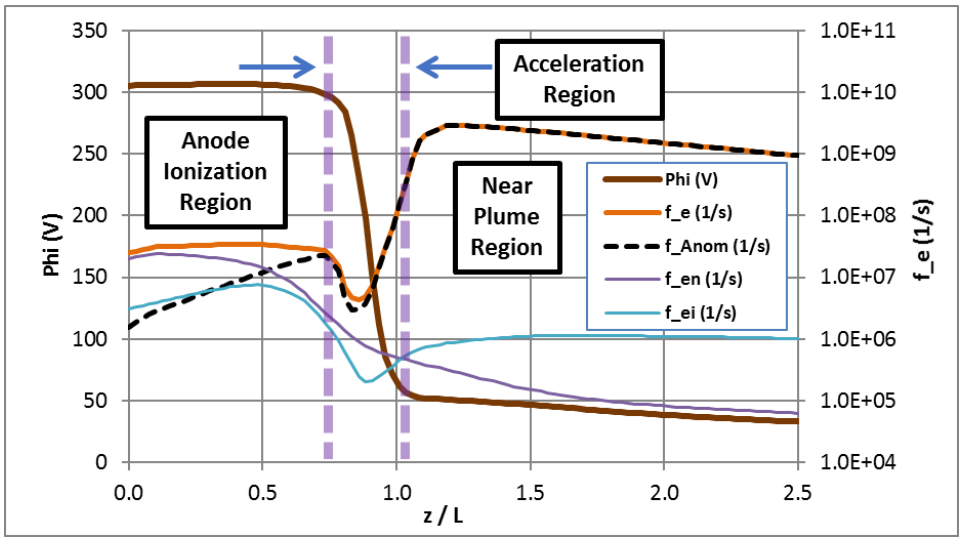

Fig. 2 The regions of a Hall thruster, shown with channel centerline potentials and electron scattering frequencies from the Hall2De 2-D, R-Z, fluid code as a function of axial distance over channel length, z/L.

Ions generated upstream in the anode ionization region are accelerated by the strong field in the acceleration region and flow at high Mach number through the near plume. Cool electrons from the thruster cathode flow upstream through the near plume. When they reach the acceleration region, they gain energy but their axial motion is severely limited by the radial magnetic field. When these hot electrons reach the gas-rich anode ionization region, they ionize the gas, become cooler, and continue drifting upstream toward the anode.

Reliance on ad hoc anomalous scattering profiles is a weakness of the Hall thruster codes that assume fluid electrons and solve for potentials using Ohm's law. To overcome this weakness, many researchers are performing one- or two-dimensional particle-in-cell simulations that resolve discrete ion and electron motion in the azimuthal dimension and solve for the potential using Poisson's equation [11-17]. These codes are designed to examine the physical processes behind "anomalous" scattering, and do not rely on any ad hoc additional scattering. By following electron and ion kinetics in the self-consistent electric fields, they show substantial electron transport across magnetic field lines. If the codes do not include classical scattering; all the cross-field transport must be produced through wave-particle scattering. It is easy to show that scattering in the azimuthal direction is necessary for electron transport across magnetic field lines [18].

In a landmark paper, Adam, Heron, and Laval [11], based on the results of a 2-D, z-θ particle simulation, proposed that turbulence generated by electron cyclotron drift instability is the cause of the enhanced cross-field electron transport observed in Hall thrusters. Electron ExB drift in the acceleration region was identified as the driving force behind the instability. The arguments were supported by both analysis and measurement. A decade later Coche and Garrigues [13] found similar results using a different 2-D, r-θ particle simulation code. Boeuf [15] presented 2-D simulations that for the first time resolved the uncorrected electron plasma frequency. These results also supported the argument that electron scattering by ion acoustic waves is the source of the anomalous cross-field transport in Hall thrusters. Later in this paper, we compare our results with those in a recent publication by Boeuf and Garrigues [16].

Over the past few years, in an attempt to make the 2-D, r-z, Hall2De code less dependent on laboratory data, we have tried to replace the ad hoc "anomalous" collision profiles with models based on quasi-linear ion acoustic wave growth rates [18,19]. This approach was successful in ORCA2D, our 2-D, R-Z hollow cathode code, where the linear growth rate for ordinary, unmagnetized, ion acoustic waves was used to calculate "anomalous" scattering [20, 21]. Our attempts to reproduce this approach in the Hall thruster code have not been satisfactory.

We found in that in the acceleration region, where the ExB drift is greatest, the quasi-linear theory of the ion acoustic instability predicts much greater electron cross-field transport than seen in Hall thrusters. Lopez Ortega [19] presented self-consistent results for the H6 thruster that agreed well with potential profiles inferred from experimental measurements [22]. In order to agree with data, this model assumes that in the acceleration region the ion acoustic instability does not enhance cross field transport. Rather, the ExB drift was limited to the order of the electron thermal speed. This condition sets a floor to the cross-field electron mobility consistent with the Buneman instability [23].

In this paper, we report on a series of numerical simulations that provide some insight into electron transport physics. The calculations presented below are for the acceleration region, with its strong electric field, and the rapid

transition to the low field, near plume region, as seen in Figure2. We have performed both 1-D azimuthal, and 2-D z-θ, PIC simulations. The intent of these calculations was to provide answers to following three questions:

What sets the location of the accelerations region?

Why is the transport lowest in the acceleration region where the electron ExB drift velocity is highest?

Why is the electric field so low in the near plume where the ExB drift is small?

III. Azimuthal Simulation in 1-D

We have run a series of PIC simulations in both 1-D and 2-D to address the disagreement between the ion acoustic enhanced transport theory and the empirically informed anomalous scattering model used in Hall2De. From Figure 2 it is clear that, downstream of the anode ionization region, classical electron transport physics is inadequate to describe Hall thruster potentials and currents. Thus, the addition of "anomalous" scattering. However, the physics of PIC codes are incorrect when classical scattering dominates. Our 1-D simulations help define the regions in a Hall thruster where PIC simulations are expected to be valid.

A. 1-D Azimuthal Calculations

Our 1-D azimuthal PIC code tracks ion and electron motion in 2-D, with a single zone in z, the axial dimension, and typically 512 azimuthal zones. The code uses a Boris algorithm for the electron Lorentz force. Xenon ions are unmagnetized. We solve Poisson's equation for the azimuthally dependent potential with periodic boundary conditions. Many of the code algorithms were benchmarked with a PIC code of Hara [12]. The cases we ran were similar to the work of Lafleur, Baalrud, and Chabert [14], but with an emphasis on the onset of ion acoustic waves in the first micro second. They showed that early there are fast moving electron waves, but soon slow moving coherent ion acoustic waves become dominant. Janhunen [17] and others have identified the source as the Electron Cyclotron Drift Instability [23, 24].

We ran simulations with the same plasma parameters for computational azimuthal dimensions ranging from 0.5 cm to 16 cm. Each of these cases, had ion acoustic waves with the same wavelength and coherence across the computational domain. The results 4 cm and 8cm domains are shown in Figure 3. Ion acoustic wave propagation is far too slow to make the waves coherent over such a large dimension in such a short time. The only explanation for the coherences is that the ion waves were initiated by the early, fast moving electron waves, the nearly vertical streaks in the first couple tenths of a microsecond (Figure 3).

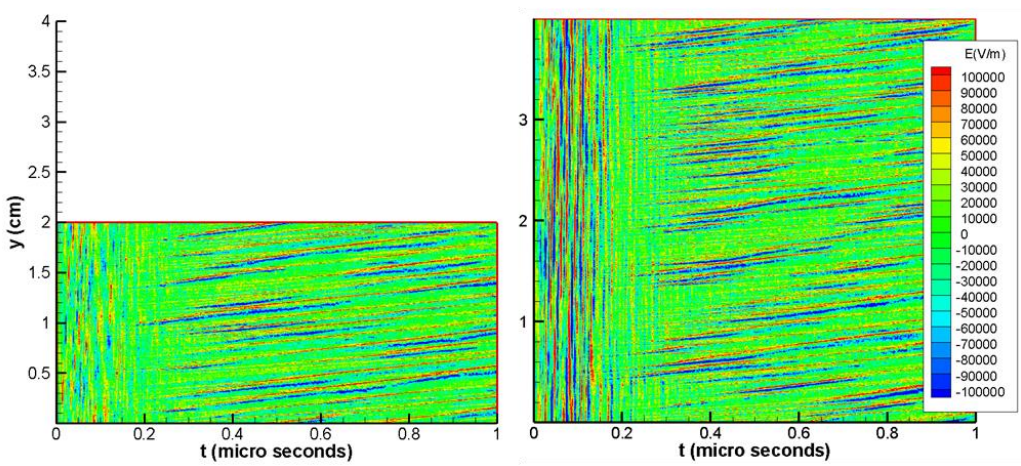

Fig. 3 Azimuthal electric field strength as a function of time for a 1-D simulations with 2 cm and 4 cm azimuthal lengths. The nearly vertical lines early on are electron waves; later on, slower moving ion waves dominate.

We are skeptical of how applicable the 1-D ion wave results are to Hall thrusters. The electron mobility calculated by the 1-D code was typically an order magnitude higher than seen is Hall thrusters. As seen in Figure 3, the azimuthal electric fields are very high, ~100 kV/m, consistent with other published 1-D simulations [14]. These high fields are

probably caused by artificial feedback due to the lack of axial variation of the potential, a problem inherent in 1-D azimuthal calculations.

B. Validity of Azimuthal Periodic Boundary Conditions

Hall thrusters are often referred to as "closed drift devices" because electrons can circumnavigate the channel without hitting a wall. The ion wave coherence across the azimuthal domain results from the coherence of the electron waves. As seen in Figure 3, electrons transit many times across the azimuthal domain before ion waves become dominant. However, electron waves will not remain coherent if the electrons were scattered by classical electron-neutral or electron ion collisions before transiting the domain.

In a Hall thruster, as shown in Figure 1, the azimuthal periodic boundary length is the circumference of the thruster channel. We introduce the ExB drift parameter, D_{ExB}, the number of times around the thruster an electron will drift before undergoing a classical scattering event, as a dimensionless measure of the electron coherence around the thruster.

$$D_{EXB} \equiv \frac{1}{2\pi\, R_{thruster}(\nu_{en} + \nu_{ei})} \cdot \frac{E}{B}$$

For coherent electron waves to develop around the channel, the drift must be the order of unity or greater.

$$D_{ExB} \gtrsim 1$$

Figure 4 shows the ExB drift parameter based on a Hall 2De calculation. The drift parameter is greater than one only in the acceleration region. Upstream of where beam ions are traveling 3000 m/s, electrons would be scattered more than ten times before they could drift around the channel circumference. The drift parameter crosses unity when the ions are moving about 6000 m/s. The drift parameter falls below one early in the near plume and remains below a tenth in the rest of the domain.

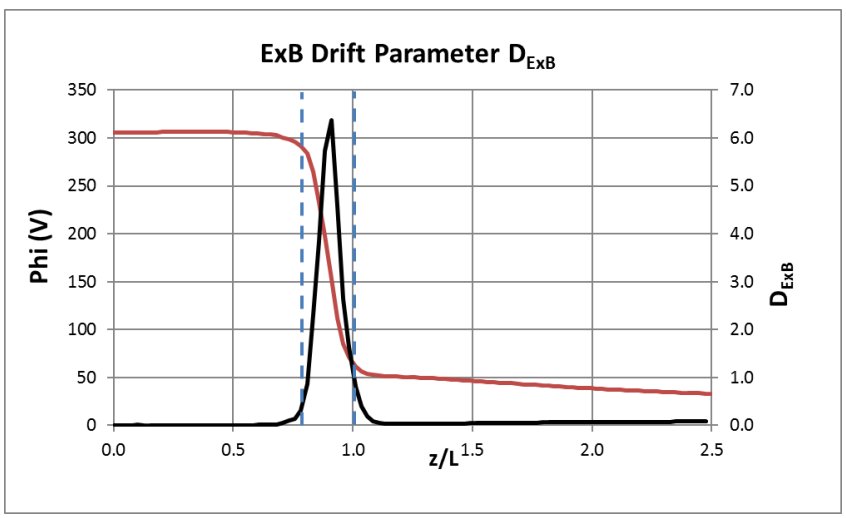

Fig. 4 The ExB Drift parameter based on a Hall2De calculation.

Previously reported 2-D, z-θ, PIC simulations [11, 13, 15, 16] included the anode ionization region. Applying azimuthal periodic boundary conditions upstream of the acceleration region enables electron wave coherence that classical scattering probably damps in real Hall thrusters. The ExB drift parameter drops well below unity downstream, suggesting that PIC results might also over predict wave amplitudes in most of the near plume region. PIC would be more valid in both these regions if simulations included classical scattering (elastic and inelastic, electron-neutral and electron-ion) and the azimuthal domain length were the order of the channel circumference.

Presently, no single computational method accurately describes Hall thruster physics in all three regions. Fluid models of both ions and electrons are good deep in the anode ionization region, where classical collisions dominate [6]. As shown above, present 2-D, z-θ, PIC codes do not adequately describe the physics in this region. Downstream, in the acceleration and near plume regions, classical collisions are less important, and the fluid and hybrid codes need ad hoc anomalous scattering profiles to model thruster behavior. 2-D, z-θ, PIC codes are applicable in the acceleration and the beginning of the near plume regions. The axial domain of the 2-D PIC calculations described in the next section, based on the ExB drift parameter arguments above, start downstream of the anode ionization region, inside the acceleration region, where beam ions have already been accelerated to 3000m/s.

IV. 2-D z-θ PIC Simulations of the Acceleration and Near Plume Region

We have developed a 2-D, z-θ, PIC code, acc2D (acceleration region 2D), to examine wave particle interactions in the acceleration and near plume regions. The code is an extension to 2-D the approach of Lafleur [14], focusing on the acceleration region and the start of the near plume region, as opposed to the full Hall thruster simulations of Adam, Coche, and Boeuf [11, 13, 15, 16]. As discussed above, our 1-D results show that PIC code physics is not appropriate upstream of the acceleration region, where the electrons scatter classically many times while drifting around the thruster circumference. Figure 5 shows the region of the Hall thruster modeled by the acc2D code. It includes most of the acceleration region and the beginning of the near plume region, the domain where $D_{ExB} \geq 1$.

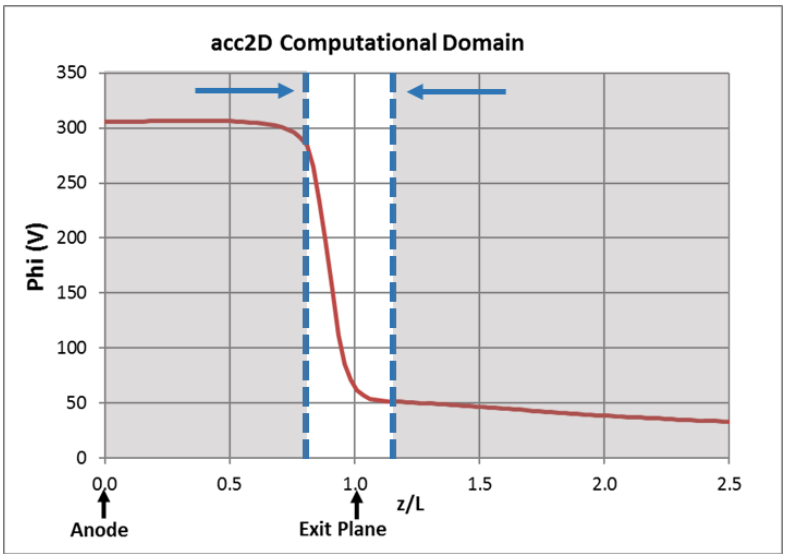

Fig. 5 The acc2D PIC code is designed the model the Hall thruster acceleration region

A. Description of the acc2D Code

The acc2D code has square cells on a planar rectilinear grid. The code ignores curvature in the azimuthal dimension. The code tracks electron and Xenon ion macroparticles of equal charge. Electron motion includes the full Lorentz force; the electric field is the only force acting on ions.

$$m_e \frac{d\mathbf{u}_e}{dt} = -e(\mathbf{E} + \mathbf{u}_e \times \mathbf{B})$$

$$m_{Xe} \frac{d\mathbf{u}_{Xe}}{dt} = e\mathbf{E}$$

The potential is obtained from Poisson's equation.

$$\nabla^2 \phi = -\frac{e}{\epsilon_0}(n_{Xe} - n_e)$$

Numerically, the potentials are node centered, the Laplacian is a 5-point stencil, and the matrix evaluated using the Intel MKL PARDISO - Parallel Direct Sparse Solver. Boundary conditions are periodic in the azimuthal direction and fixed on axial boundaries. In all the cases reported below, the upstream potential was 225V and the downstream (cathode) potential was 0V. The total voltage drop, shown in Figure 5, is representative of a 300V Hall thruster.

Table 1 shows code parameters for the cases reported here. The magnetic field was parabolic in the axial direction, peaking at the middle of the grid. The grid spacing was adequate to resolve the Debye length throughout the domain. At the downstream end of the grid, the electrons are cold (2eV) and, because the ions have been accelerated, the density drops to 8×10^{16} m^{-3}. Near the upstream boundary the electron energies become high, and the effective Debye length is longer.

Table 1 Parameters used in the acc2D calculations

Parameter	Value
z length	10 mm
y length	2.5 mm
Nz	500
Ny	125
$\Delta z, \Delta y$	2×10^{-5} m
n_{i0}	4×10^{17} m^{-3}
u_{i0}	3000 m/s (6.2 eV)
j_{i0}	200 A/m^2
T_{i0}	0.1 eV
T_{e0}	2 eV
NG	32
Δt	2.5×10^{-12} s
φ_{anode}	225 V
$\varphi_{cathode}$	0 V
B_{max}	200 G
B_{min}	100 G

Ions are seeded uniformly in the azimuthal direction. Axially, the ions are seeded with spacing and velocities consistent with a linear potential drop from upstream to downstream. Each ion starts with a collocated, zero velocity electron. On the average, there are 32 macro particles of each species per cell in a grid space 4 azimuthally by 8 axially. The calculations reported typically had about 4 million macro particles, 2 million of each species. We ran one case with three times the number of macro particles and saw little difference in results. We have not done the extensive sensitivity testing reported in Reference 16.

After every 93 timesteps, four ion macroparticles were added, uniformly spaced azimuthally, to each cell along the upstream boundary. During the calculation, an anode sheath develops at the upstream boundary. To prevent ions from being reflected out the anode, the ion axial velocity was never allowed to drop below the injection velocity. In the cases shown here, the ion injection velocity is 3000 m/s, corresponding to an initial kinetic energy of 6 eV. Added to this axial velocity are random axial and azimuthal velocity components consistent with a 0.1 eV ion temperature. Ions have periodic boundary conditions azimuthally and are lost from the system when they leave through the downstream boundary. The code can also introduce ion and electron pairs inside the domain to simulate ionization.

Electron are injected at the downstream boundary only when the potential in a cell along that boundary is positive enough, 0.05 V, that adding a macro particle electron to the cell doesn't make the potential go negative. This injection criterion enables both fixed potential ($\varphi_{downstream}$ =0 V) and fixed electric field ($E_{downstream}$ = 0) boundary conditions downstream. As with ions, electrons have periodic boundary conditions azimuthally. If electrons leave axially through either the upstream or downstream boundaries, they are lost from the system.

Major code outputs include the azimuthally averaged potential profile, the ratio of electron current to ion current, the electron and ion velocity distribution functions, and the azimuthal wave electric field amplitudes. The ratio of electron current to ion current is the key measure of cross-field transport. For example in Hall2de, the ad hoc anomalous collision frequency profile is iterated until the code reproduces the measured anode current while matching the thrust and mass flow rate. Anode current is the sum of electron and ion currents across the acceleration region. The ion current is controlled mainly by the gas flow rate (propellant utilization is >90%). The PIC code calculates electron current by counting the macro particles that exit the grid at the upstream boundary..

B. 2-D Calculation: Beam Ions Only

For the parameters in Table I, a xenon ion transits the system in about a microsecond. We have run a case with beam ions only for seven microseconds. There was little change to the calculated potentials or electron currents after a microsecond. Figure 6 shows the potential profile at seven microseconds plotted along with the magnetic field profile.

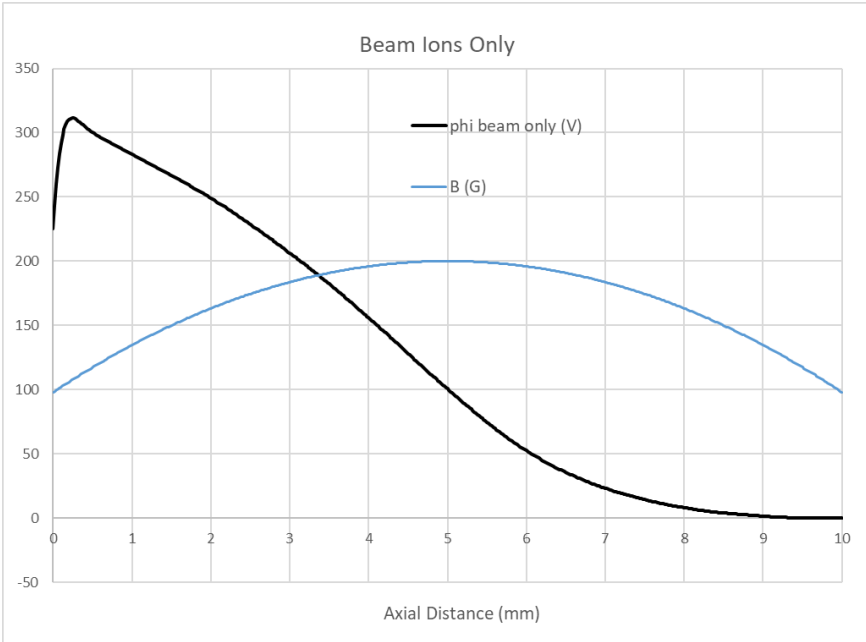

Fig. 6 Baseline potential profile after seven microseconds.

The potential profile has features near both the upstream and downstream boundaries. The electron emission algorithm keeps the electric field near zero at the downstream boundary. At the upstream boundary, there is a large, 100 V, anode sheath. This sheath forms because the electron current throughout the grid is severely magnetically limited, and the electrons near the upstream boundary are quite hot. Electrons gain energy as they move up the potential, and there are no collisional energy loss mechanisms. The potential drop extends across the entire computational domain, suggesting that if the domain were larger, the potential would keep expanding. This calculation gives no insight into why the acceleration regions in real Hall thrusters are so short.

After a startup transient in the first microsecond, the electron current remained relatively stable as shown in Figure 7. In a Hall thruster, the electron current is typically about 30% of the ion current. In this calculation, over the last several microseconds, the electron current was only about 2.5% of the ion current, an order of magnitude low, indicating there was not enough cross-field transport. Clearly, there was something missing in the calculation.

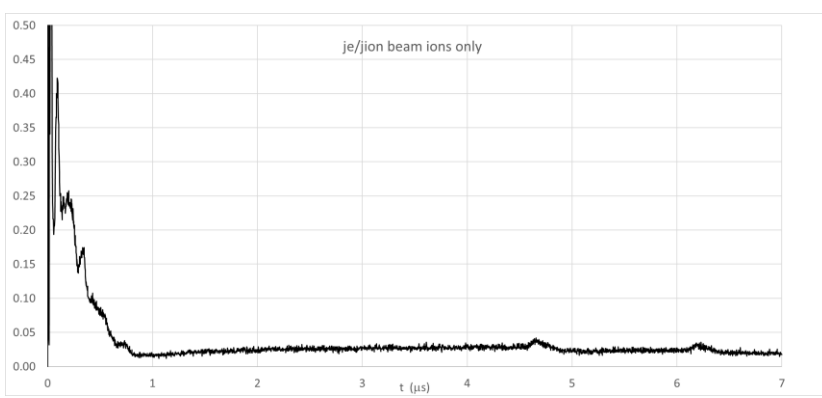

Fig. 7 Ratio of electron current to ion beam current in the baseline calculation

We ran a case with the same parameters, but with a constant, 150G, magnetic field. The potential profile was very similar. There was somewhat more electron current (je/jion ≈ 4.2%), still almost an order of magnitude below that in typical Hall thrusters.

C. Calculations with Ionization

We examined the Hall2De calculation results to see what was missing in the baseline calculation. Figure 1 shows that classical scattering is unimportant in the acceleration and near plume regions. While ionization peaks in the anode ionization region, upstream of the acceleration region, Hall2De results showed that ionization amounting to about a tenth of the beam current takes place in our PIC domain. To test the importance of downstream ionization, we added a constant cold ion generation rate throughout the entire computational domain, except for the anode sheath. The rate chosen was from near the end of the acceleration region in the Hall2De calculation and increased the total ion current by less than 6%. Each ion and electron pair was born with zero velocity. To prevent artificially stimulating azimuthal waves, after every 40,000 timesteps, a single ion and electron pair was placed in every azimuthal cell in every fifth axial row of cells. This prevented any azimuthal density variation due to the emission process.

With this small amount (6%) of additional cold ions and electrons, the PIC code results were much different. The potential profile was no longer a smooth curve that spans the entire length of the grid, but has broken into two distinct regions. As shown in Figure 8, the entire potential drop is constrained to the upstream half of the grid. The potential is flat in the downstream half of the grid. There is a rapid transition between the two regions, similar to the transition between the acceleration and the near plume regions in a Hall thruster

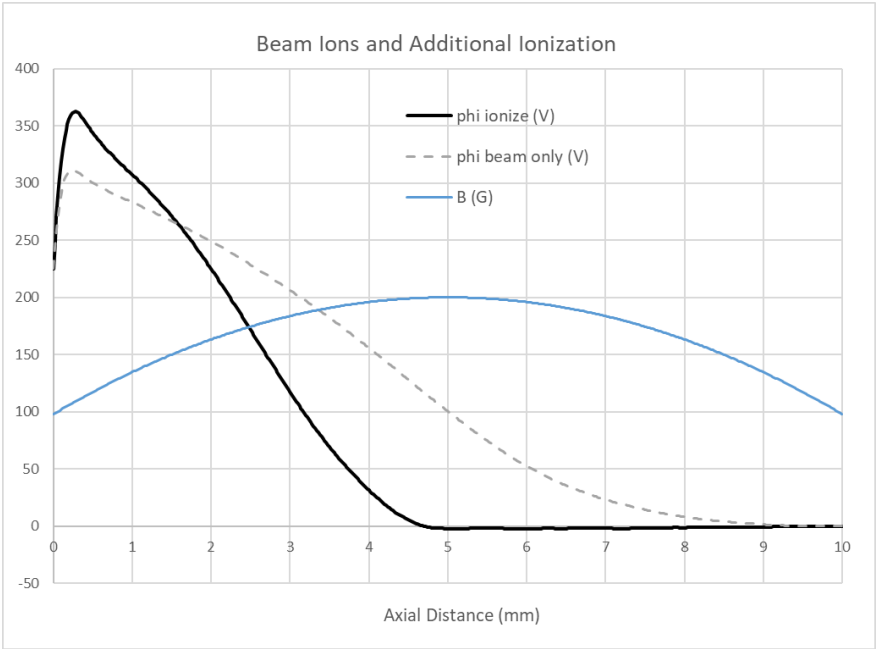

Fig. 8 Potential profile for case with a small amount of ionization compared with the baseline, both after seven microseconds.

The time evolution of the electron current was also much different. Not only was the magnitude greater, about a fourfold increase, but a quasi-periodic behavior appeared as seen in Figure 9.

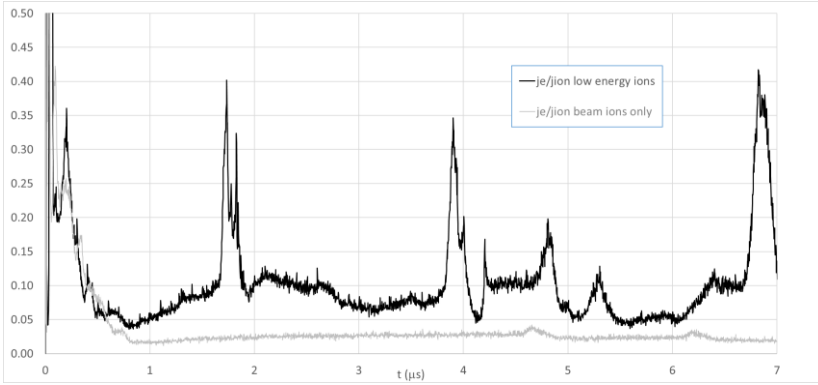

Fig. 9 Ratio of electron current to ion beam current as a function of time for the case with a small amount of ionization compared with results from the baseline calculation.

The electron azimuthal velocity distribution, shown in Figure 10, becomes very non-Maxwellian as the electrons move upstream from the downstream boundary. Even though the electric field is small in the downstream half of the domain, z > 5 mm, the electrons are heating, as seen in Figure 10. The electrons enter downstream, z=10 mm, with a temperature of 2eV. By the time they have traversed a quarter of the domain, z=7.5 mm, they have a kinetic energy greater than 10 eV. Further upstream the distribution function becomes increasingly non-Maxwellian. In the upstream half of the domain, the average electron kinetic energy becomes quite large (Figure 11). Most of this energy is from the ExB drift. With this steep potential profile, the ExB drift velocity peak is 6.4×10^6 m/s at 2.5 mm, corresponding to a kinetic energy greater than 115 eV and accounts for most of the electron kinetic energy.

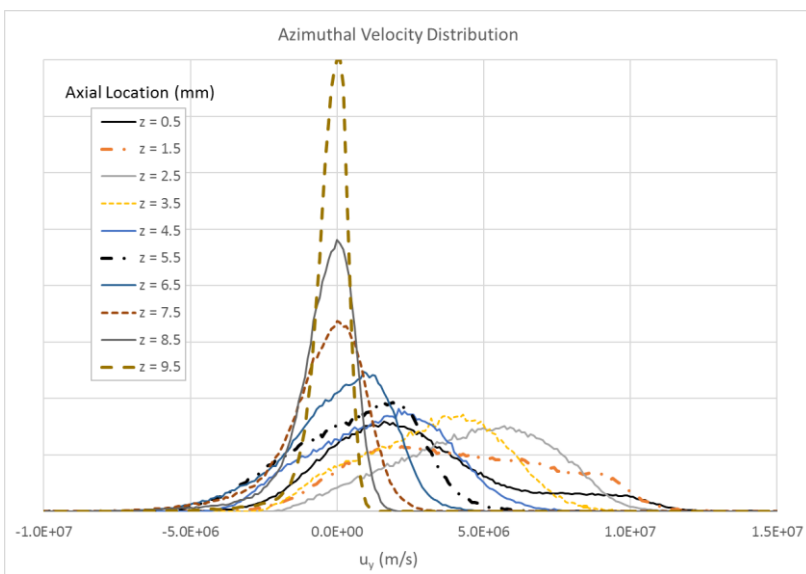

Fig. 10 Electron azimuthal velocity distribution after 7 μs at different axial locations for the case with ionization.

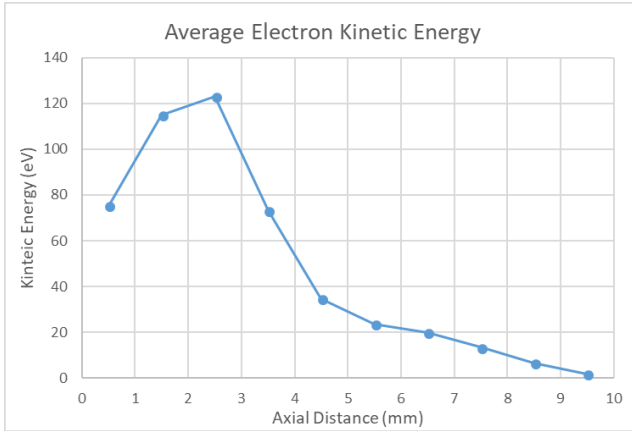

Fig. 11 Average electron kinetic energy as a function of axial position for the base case with ionization. Most of the kinetic energy in the upstream half of the domain is from the ExB drift velocity

V. Analysis of the numerical results

The most surprising result from the 2-D calculations was that with a small, realistic, amount of ionization, the potential in the computation domain split into two distinct regions, an upstream region that contained the total potential drop, and a downstream region where the potential was very flat. We performed several other calculations with and without ionization and they all showed the same behavior. Figure 12 shows results from calculations with four different ionization profiles and the same magnetic field profile compared with the no ionization base case. Included are the uniform ionization case described above, ionization only where the potential is less than 50V, five times the ionization, and a more realistic ionization profile based on the reference Hall2De calculation scaled down by the beam current density (PIC $j_{beam} \approx 200 A/m^2$, Hall2De $j_{beam} \approx 800 A/m^2$). In every case with ionization, the potential in the downstream half of the computational region is flat. The extent of the flat region was shortest in the case with the least ionization, ionization only below 50V, and longest in the case with the most ionization, 5X. Examining the code diagnostic output has given us clues to the relevant physics in the two regions.

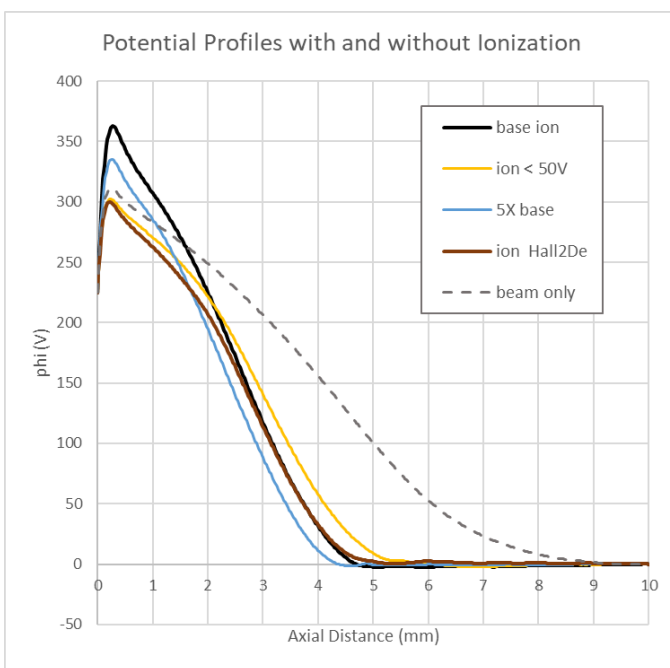

Fig. 12 Potential profiles for cases run with four different ionization profiles compared with the base case of beam ions only and no ionization. All cases with ionization resulted in flat downstream potentials.

Electrons flow upstream from the downstream boundary, yet, for all cases with ionization, the potentials in Figure 12 are essentially flat in the downstream half of the domain. The magnetic field in this region varies between 100G and 200G, the Larmor radius of 2eV electrons is a few tenths of a millimeter, and yet the current flows as if the electrons were not magnetized. Why?

In a fluid code, like Hall2De, the magnetic field enters Ohm's law, the electron momentum equation, through the classical Hall parameter.

$$\Omega_{class} \equiv \frac{\omega_{ce}}{(\nu_{en} + \nu_{ei})} = \frac{eB}{m_e(\nu_{en} + \nu_{ei})}$$

The Hall parameter measures the importance of the magnetic field on electron transport. When $\Omega_{class} < 1$, the magnetic field has little effect on electron currents; when $\Omega_{class} > 1$, the magnetic field limits cross-field transport.

The 2-D PIC code solves only a few equations: electron and ion equations of motion, and Poisson's equation for the potential. The magnetic field enters only in electron momentum equation.

$$m_e \frac{d\mathbf{u}_e}{dt} = -e(\mathbf{E} + \mathbf{u}_e \times \mathbf{B})$$

In the azimuthal direction, the only electric field is from waves.

$$m_e \frac{du_\theta}{dt} = -e(E_{wave} + u_z B)$$

The ratio of the two terms on the right hand side is a measure of the importance of the magnetic field on electron motion, analogous to the classical Hall parameter.

$$\Omega_{anom} \equiv \frac{u_z B}{E_{wave}}$$

Notice that the higher the electron velocity, the more important the magnetic field. If Ω_{anom} is small, the magnetic field has little effect on electron transport; the electrons are "unmagnetized".

A contour map of the instantaneous azimuthal electric field from the base case with ionization is shown in Figure 13. The RMS average of the field over the downstream half of the grid is

$$\sqrt{\langle E_y^2 \rangle} = 3500 \frac{V}{m}.$$

The corresponding potential fluctuations are less than a volt.

$$\sqrt{\langle \phi^2 \rangle - \langle \phi \rangle^2} = 0.3\ V$$

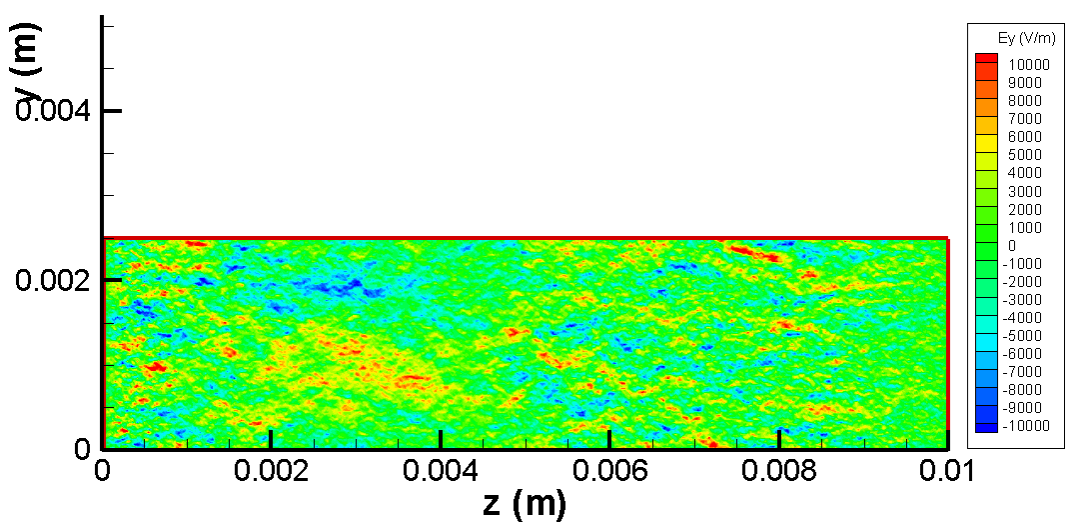

Fig. 13 Azimuthal electric field from the calculation with ionization.

The anomalous Hall parameter is less than one for electrons with velocities less than

$$u_z < \frac{E_{wave}}{B} \approx 2.3 \times 10^5 \frac{m}{s} \implies \Omega_{anom} < 1\,.$$

The ion density throughout the domain is shown in Figure 14. The density striations are normally associated with ion waves, the probable source of the electric field fluctuations seen in Figure 13.

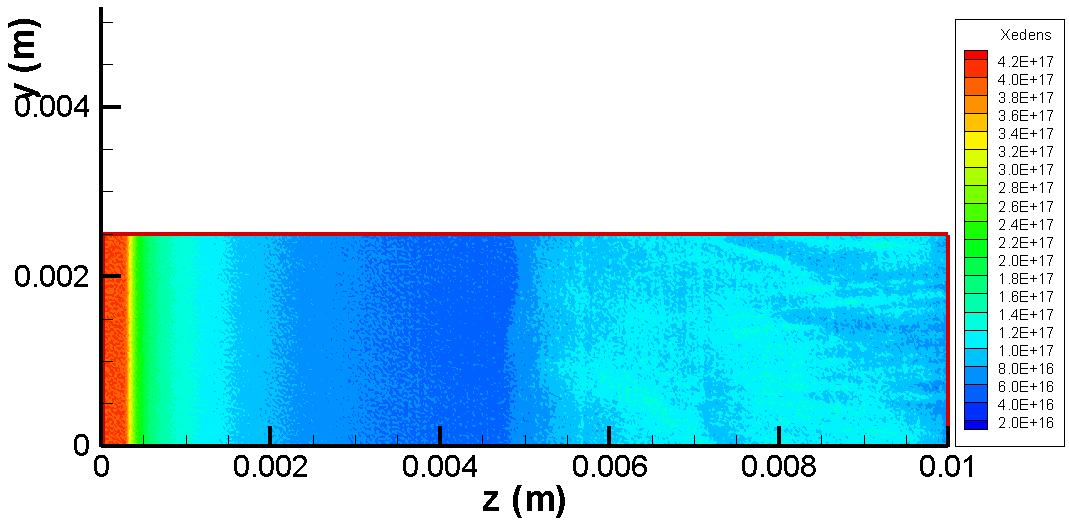

Fig. 14 Xenon ion density corresponding to the azimuthal electric fields in Figure 11.

At the downstream boundary, where T_e = 2eV, a significant fraction of the electrons have axial velocities low enough for $\Omega_{anom} < 1$. As electrons move upstream and are heated, the unmagnetized fraction drops. To carry the calculated electron current, the average electron drift velocity near the downstream boundary is only about 5000 m/s, the electron thermal speed is about 600,000 m/s. So only a very small fraction of the electrons need to act as if unmagnetized.

The following picture emerges from the calculations. In steady (or quasi-steady) state, everywhere in the system where classical collisions are small, ion waves with significant azimuthal electric fields are present. These electric fields and their related potential fluctuations are relatively small relative to the electron energies and axial electric fields in the acceleration region.

Downstream, in the near plume, the electron energies and temperatures are low and enough electrons are unmagnetized,

$$\Omega_{anom} = \frac{u_z B}{E_{wave}} < 1 \,,$$

to carry the required electron current. The classical collision frequency is also low (zero in the PIC code), so the resistivity is low, thus the axial electric fields are low.

Electrons start gaining energy as they approach the acceleration region. As the electron velocities increase, the trajectories of more and more are dominated by the magnetic field, $\Omega_{anom} > 1$. At some point the wave energy is not high enough to keep all current carrying electrons unmagnetized. This increases the axial electric field required pull in the electrons, which in turn further increases the azimuthal velocities. This makes more electrons magnetized.

$$\Omega_{anom} = \frac{u_z B}{E_{wave}} > 1$$

In this region, the resistivity is high.

As the electrons move upstream into the anode ionization region (not included in the PIC calculations), classical collisions become important. The average electron energy decreases due to ionization losses. There can still be some ion acoustic waves, but for most of the region, classical collisions dominate. The ions and electrons start to behave as fluids. For much of this region the combined Hall parameter is low,

$$\Omega_{total} \approx 1 \,,$$

and plasma resistivity and electric fields are low.

The analysis above suggests that electron kinetic energy is what separates the three regions. The temperature profile calculated by Hall2De, Figure 15, is consistent with this picture. The general concept is that the electron current density in Hall thrusters is a tiny fraction of the electron thermal flux. In the examples above, the electron current density is at most 2% of the electron one-sided thermal flux. The small fraction of cool electrons that carry current in the near plume are “unmagnetized” because of scattering by low amplitude waves. As their kinetic energy increases, they reach a point where magnetic effects become important, requiring higher electric fields, that in turn increases their energy, and so on. Upstream, ionization and classical collisions cool the electrons, and again they behave as if “unmagnetized”.

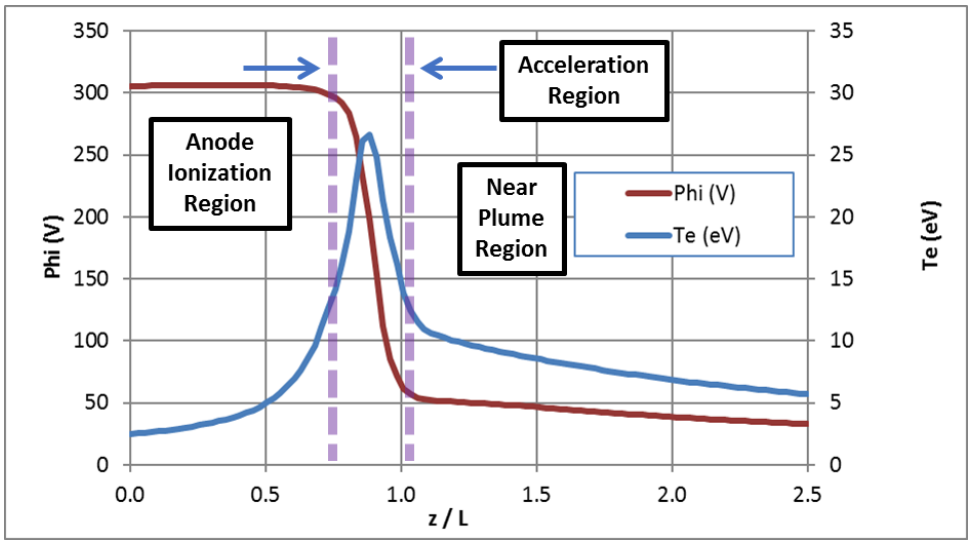

Fig. 15 The acceleration region is a region with hot electrons between two plasmas with cooler electrons.

Models based on wave growth in isothermal, homogeneous plasmas do not capture this behavior, which appeared in our calculations only after the inclusion of ionization in the domain. Ionization created a low energy plasma component in the downstream half of the domain. This plasma has both high speed beam ions and low speed ions. High speed beam ions convect their density fluctuations out of the domain in less than a microsecond. The ions with low axial speed take longer to leave the domain, as does their wave energy. The wave energy in the downstream half of the grid is not the result of any local ExB drift; the axial electric field there is near zero. Rather, it appears that some of the ExB wave energy generated in the high field, upstream region, is transferred by beam ions to the downstream low energy ion population created by ionization.

VI. Comparison with results of Boeuf and Garrigues

Boeuf and Garrigues (BG) [16] presented results from their 2-D, z-θ PIC code that they suggested could "serve as benchmarks for comparisons between different simulation codes." The calculations presented above, while similar in many ways to their results, have significant differences that lead to differing conclusions. The 2-D results presented above are most comparable with their case with ion mass current density $J_M = 200\ A/m^2$ and 40 particles per cell.

The parameters for our 2-D PIC calculations were chosen based on experimentally validated results from a Hall2De simulation. While Hall2De relies on an ad hoc anomalous scattering profile, when fit using a few experimental parameters, it accurately predicts thruster plasma properties.

The most significant difference is the axial extent of the calculation domain. The Boeuf and Garrigues computational domain includes the entirety of the anode ionization region. As shown above the ExB drift parameter is small, $D_{ExB} \ll 1$, in this region and periodic azimuthal boundary conditions are incorrect. The calculations above start when drift parameter becomes the order of unity, $D_{ExB} \approx 1$.

The axial extent determines the upstream boundary condition. Since all of the ionization is included in the BG domain, no ions enter upstream, ions can exit both upstream and downstream. In agreement with LIF measurements of on modern, high efficiency, Hall thrusters [22, 25], Hall2De results show almost 90% of the thruster beam ion current is generated upstream of the acceleration region. BG show about 50% of the ionization occurring in the acceleration region, and ion energy distribution functions with a large low velocity tail. The published LIF measurements for 300V Hall thrusters show no significant low energy tail.

BG recognized that "the conditions of the simulations are not those of a real Hall thruster (smaller magnetic field, imposed position and profile of the ionization source, etc.)". The conditions in the 2-D PIC simulations presented attempt to remedy some of these shortcomings by using the Hall2De results as a guide. But the simulations presented are far from perfect. The radial magnetic field profile used, while of the right magnitude, 200G, has an arbitrary profile. To shorten run times, the ion current density, $j_{beam} = 200\ A/m^2$ is a only quarter that in the Hall2De calculations.

BG performed extensive numerical sensitivity studies, far more than have been done on the code reported on in this paper.

A critical parameter in Hall thrusters is the electron current compared with the ion current. For the Hall2De case used to baseline our simulations $\frac{j_e}{j_i} \approx 30\%$. For the case above with a low, uniform ionization profile, the ratio was 10%. With a more realistic ionization profile, the ratio increased to 19%. In the BG results, where almost half the ionization was in the acceleration region, the ratio was about 65%. Both BG and our results are consistent with the analysis above that increased ionization in the acceleration and near plume regions lead to increased electron transport. BG attributed the transport increase to the increase in total ion current. Because we also ran cases with no ionization and high energy beam ions only, we are able to identify low energy ions produced by ionization in the acceleration and near plume regions as the dominant source of enhanced electron transport.

VII. Conclusion

Over the past two decades, 2-D r-z, fluid codes have been remarkably successful in advancing of Hall thrusters design and engineering. For example, Hall2De led to the understanding of magnetic shielding [9,10] and is being used in the design and development of the HERMeS thruster [26]. However, the fluid models don't describe the physics of electron transport. They calculate the potentials and electron temperatures using fixed spatial "anomalous scattering" profiles, informed by experiment, in Ohm's law. The experimental data includes LIF used to locate the acceleration region.

More recently, 2-D z-θ PIC models have been applied to Hall thrusters. The code results have successfully reproduced qualitatively many features of Hall thruster plasmas. However, the physics in z-θ PIC codes are only applicable to a small fraction of the Hall thruster domain. Geometrically, these codes are more comparable to 1-D axial fluid or hybrid codes than 2-D r-z codes like Hall2De. Codes like Hall2De represent Hall thruster geometry accurately enough to be used as engineering design and analysis tools. The objective of the study presented above is to learn more about the physics controlling electron transport, so we can replace the ad hoc "anomalous scattering" model in Hall2De with a model better grounded in physics.

A previous attempt at such an "anomalous scattering" model [18, 25] included a couple of features confirmed by the calculations above. First, only when the classical electron azimuthal scattering length is long can the effective Hall parameter become large. Second, plasma waves in the acceleration region are ineffective at scattering the hot electrons there. These electrons are accelerated by the high axial electric fields. In regions dominated by cooler, more Maxwellian electrons, plasma waves are effective at allowing cross-field transport and axial electric fields are small. The model in Ref. 18 had enhanced transport starting downstream the peak magnetic field. The calculations above suggest greatly enhanced transport starts where the average electron energy drops below some critical value. In future work, we intend to apply the insight gained from our PIC simulations in developing better transport models for the fluid code.

Acknowledgments

The authors would like to acknowledge the contributions of Dr. Ioannis G. Mikellides and Prof. Benjamin A. Jorns, whose work set the foundations for the model presented in this article. We would like to thank Dr. Dan M. Goebel for his help reviewing and revising this paper. We would like to thank Prof. Kentaro Hara for contribution during the development and benchmarking of the PIC codes reported here. The research described in this paper was carried out by the Jet Propulsion Laboratory, California Institute of Technology, under a contract with the National Aeronautics and Space Administration. The support of the joint NASA GRC and JPL development of the Advanced Electric Propulsion System by NASA's Space Technology Mission Directorate through the Solar Electric Propulsion Technology Demonstration Mission project is gratefully acknowledged.

References

[1] Fife, J. M., "Hybrid-PIC Modeling and Electrostatic Probe Survey of Hall Thrusters," Ph.D. Thesis, Aeronautics and Astronautics, Massachusetts Institute of Technology, 1998

[2] Fife, J. M., Martinez-Sanchez, M., and Szabo, J., "A Numerical Study of Low-Frequency Discharge Oscillations in Hall Thrusters," *33rd AIAA/ASMA/SAE/ASEE Joint Propulsion Conference*, Seattle, WA, 1997.

[3] Boeuf, J. P., and Garrigues, L., "Low Frequency Oscillations in a Stationary Plasma Thruster," *Journal of Applied Physics*, 84, 7, p. 3541, 1998.

[4] Hagelaar, G., Bareilles, J., Garrigues, L., and Boeuf, J. P., "Two Dimensional Model of a Stationary Plasma Thruster," *Journal of Applied Physics*, 91, p. 5592, 2002.

[5] Bareilles, J., Hagelaar, G., Garrigues, L., Boniface, C., and Boeufa, J., "Critical Assessment of a Two-Dimensional Hybrid Hall Thruster Model: Comparisons with Experiments," *Physics of Plasmas*, 11, 6, 2004.
[6] Mikellides, I. G. and Katz, I., "Numerical Simulations of Hall-effect Plasma Accelerators on a Magnetic-Field-Aligned Mesh", *Physical Review E*, Vol. 86, 2012, p. 046703
[7] Gamero-Castaño, M. and Katz, I., "Estimation of Hall Thruster Erosion Using HPHall," *29th International Electric Propulsion Conference*, IEPC Paper 2005-303, Princeton, NJ, 2005.
[8] Hofer, R. R., Mikellides, I. G., Katz, I., and Goebel, D. M., "BPT-4000 Hall Thruster Discharge Chamber Erosion Model Comparison with Qualification Life Test Data," *30th International Electric Propulsion Conference*, IEPC Paper 2007-267, Florence, Italy, 2007.
[9] Mikellides, I. G., Katz, I., Hofer, R. R., Goebel, D. M, de Grys, K., and Mathers, A., "Magnetic shielding of the channel walls in a Hall plasma accelerator", *Physics of Plasmas* 18, 033501 2011
[10] Mikellides, I. G., Katz, I., Hofer, R. R., and Goebel, D. M., "Magnetic Shielding of a Laboratory Hall Thruster. I: Theory and Validation," *Journal of Applied Physics*, Vol. 115, 2014, pp. 043303
[11] Adam, J. C., Heron, A., and Laval, G., "Study of Stationary Plasma Thrusters Using Two-dimensional Fully Kinetic Simulations", *Physics of Plasmas*, Vol. 11, 2004, 295
[12] K. Hara and S. Cho, "Radial-azimuthal particle-in-cell simulation of a Hall effect thruster," IEPC-2017-495, 35th *International Electric Propulsion Conference*, Atlanta, GA, October 2017
[13] Coche, P. and Garrigues, L., "A Two-Dimensional (Azimuthal-Axial) Particle-In-Cell Model of a Hall Thruster", *Phys Plamas* 21, 023503, 2014
[14] Lafleur, T., Baalrud, S. D. and Chabert, P., "Theory for the anomalous electron transport in Hall effect thrusters. I. Insights from particle-in-cell simulations", Physics of Plasmas 23, 053502 (2016)
[15] Boeuf, J.P., "New insights from PIC simulations on the EXB Electron Drift Instability in Hall thrusters", *35th International Electric Propulsion Conference*, IEPC-2017-216
[16] Boeuf, Jean-Pierre & Garrigues, L. (2018). E × B electron drift instability in Hall thrusters: Particle-in-cell simulations vs. theory. Physics of Plasmas. 25. 061204
[17] Janhunen, S., Smolyakov, A., Chapurin, O., Sydorenko, D., Kaganovich, I., and Raitses, Y., "Nonlinear structures and anomalous transport in partially magnetized ExB plasmas", *Physics of Plasmas* 25, 011608, 2018
[18] I. Katz, I. G. Mikellides, A. J. Jorns, and A. Lopez-Ortega, "Hall2De simulations with an anomalous transport model based on the electron cyclotron drift instability," *34th International Electric Propulsion Conference* (Kobe, Japan, 2015), IEPC-2015-402
[19] Lopez Ortega, A., Katz, I. and Chaplin, V.H., "A First-Principles Model Based on Saturation of the Electron Cyclotron Drift Instability for Electron Transport in Hydrodynamics Simulations of Hall Thruster Plasmas", *35th International Electric Propulsion Conference*, IEPC-2017-178
[20] Lopez Ortega, A., Mikellides, I. G., and Jorns, B. A., "First-principles Modeling of IAT-driven Anomalous Resistivity in Hollow Cathode Discharges II: Numerical Simulations and Comparisons with Experiments", AIAA paper No. 2016-4627, July 2016.
[21] Lopez Ortega, A., Mikellides, I. G., and Jorns, B. A., "Hollow Cathode Plasma Simulations with a First-principles Model of IAT-driven Anomalous Resistivity", submitted to Journal of Propulsion and Power, 2017.
[22] Huang, W., Drenkow, B., and Gallimore, A.D., "Laser-Induced Fluorescence of Singly-Charged Xenon inside a 6-kW Hall Thruster", *45th AIAA/ASME/SAE/ASEE Joint Propulsion Conference & Exhibit*, AIAA 2009-5355
[23] Buneman, O., "Instabillty of Electrons Drifting Through Ions Across a Magnetic Field", *Plasma Physics (Journal of Nuclear Energy Part C)* 1962, Vol. 4, pp, 111 to 117
[24] D. W. Forslund, R. L. Morse, and C. W. Nielson, "Electron Cyclotron Drift Instability", *Phys. Rev. Lett*. 25, 1266 (1970).
[25] Chaplin, V. H., Jorns, B. A., Conversano, R. W., Lobbia, R. B., and Lopez Ortega, A., "Laser Induced Fluorescence Measurements of the Acceleration Zone in the 12.5 kW HERMeS Hall Thruster", IEPC-2017-229, October 2017
[26] Hofer, R. R., Polk, J. E., Sekerak, M. J., Mikellides, I. G., Kamhawi, H., Sever-Verhey, T. R., Herman, D. A., and Williams, G., "The 12.5 kW Hall Effect Rocket with Magnetic Shielding (HERMeS) for the Asteroid Redirect Robotic Mission", AIAA paper 2016-4825, July 2016
[27] Lopez Ortega, A., Katz, I. and Chaplin, V.H., "Application of a first-principles anomalous transport model for electrons to multiple Hall thrusters and operating conditions", *2018 Joint Propulsion Conference, AIAA Propulsion and Energy Forum and Exposition*, Cincinnati, OH, July 2018